

IONIZATION RATE AND PLASMA DYNAMICS AT 3.9 MICRON FEMTOSECOND PHOTOIONIZATION OF AIR

Adam Patel¹, Claudia Gollner², Rokas Jutas², Valentina Shumakova², Mikhail N. Shneider,³ Audrius Pugzlys²,
Andrius Baltuska², and Alexey Shashurin¹

¹ *School of Aeronautics and Astronautics, Purdue University, West Lafayette, IN, USA*

² *Photonics Institute, Vienna University of Technology, Vienna, Austria*

³ *Mechanical and Aerospace Engineering, Princeton University, Princeton, NJ, USA*

Abstract

The introduction of mid-IR optical parametric chirped pulse amplifiers (OPCPAs) has catalyzed interest in multi-millijoule, infrared femtosecond pulse-based filamentation. As tunneling ionization is a fundamental first stage in these high-intensity laser-matter interactions, characterizing the process is critical to understand derivative topical studies on femtosecond filamentation and self-focusing. Here, we report first direct nonintrusive measurements of total electron count and electron number densities generated at 3.9 μm femtosecond mid-infrared tunneling ionization of atmospheric air using constructive-elastic microwave scattering. Subsequently, we determine photoionization rates to be in the range of $5.0 \times 10^8 - 6.1 \times 10^9 \text{ s}^{-1}$ for radiation intensities of $1.3 \times 10^{13} - 1.9 \times 10^{14} \text{ W/cm}^2$, respectively. The proposed approach paves the way to precisely tabulate photoionization rates in mid-IR for broad range of intensities and gas types and to study plasma dynamics at mid-IR filamentation.

Corresponding author: Alexey Shashurin ashashur@purdue.edu

Introduction. - Strong field ionization of gases by intense femtosecond laser pulses enables a plethora of frontier fundamental research fields in nonlinear optics, such as high-order harmonic generation (HHG) and attosecond science,¹ femtosecond filamentation,^{2,3} standoff nonlinear spectroscopy of atmosphere,⁴ etc. In contrast to optical breakdown triggered by picosecond (and longer) laser pulses or microwave discharges (where Joule heating of photoelectrons and avalanche ionization play a major role in evolution of the plasma, density, temperature, and energy/momentum distribution of photoelectrons), plasmas generated by femtosecond pulses in atmospheric pressure gases are fully determined by the fundamental quantum process of strong field ionization. Very recent progress in the development of high-energy femtosecond laser systems in the mid-infrared (mid-IR) spectral range has opened new regimes and perspectives in strong field physics and femtosecond filamentation.^{5,6,7,8,9} Specifically, these refer to the increased propagation range of the mid-IR laser radiation through the atmosphere in comparison to their traditional near-IR counterparts and, therefore, enable a variety of applications including remote sensing of the atmosphere, free-space communications, directed energy applications, and laser propulsion for deep-space travel.^{4,5,6,7,8,10,11}

Accurate knowledge of the plasma properties, generated by intense ultrashort mid-IR laser pulses, and their dependence on laser pulse parameters has critical importance for understanding physics and the precision of numerical simulations of HHG and generation of attosecond pulses, laser wake-field acceleration,¹² femtosecond filamentation, and related phenomena like standoff terahertz emission generation,¹³ laser-controlled weather phenomena,¹⁴ standoff lasing,^{4,15} etc. The dependence of ionization rate on laser intensity and wavelength for atomic gases was theoretically described in seminal works.^{16,17,18} In the latest development of these theoretical models, it was shown that the ionization probability as well as the momentum and energy distributions of photoelectrons are strongly affected by the laser wavelength and polarization.¹⁹ However, even for atomic gases, there are no absolute measurements of the plasma parameters and ionization rates generated by the laser pulse in mid-IR, and experiments conducted thus far are mostly in a narrow spectral range of 0.8-1 μm with near-IR lasers, providing semi-empirical agreement with theoretical predictions.^{20,21} The status quo in molecular gases, demonstrating additional strong dependence of ionization on molecular orientation and internal ultrafast dynamics,^{22,23} is even worse and, despite extensive theoretical efforts to extend atomic strong field ionization models to molecules,²⁴ simulations and experiments currently rely on empirical dependences retrieved for a limited range of intensities and for particular laser wavelengths.^{25,26,27}

Measurements of absolute electron numbers generated in gases by intense femtosecond laser pulses and corresponding photoionization rates are very challenging. For relatively high plasma densities, $n_e \geq 10^{16} \text{ cm}^{-3}$ methods of optical interferometry or shadowgraphy can be employed.^{28,29} However, the ionization rate is predicted to drop with increasing laser wavelength,⁵ and methods for electron density measurements in mid-IR filaments below the limit of $n_e \leq 10^{16} \text{ cm}^{-3}$ are required. A number of semi-empirical and/or indirect methods was proposed, including ion current measurement

by time-of-flight mass spectrometer, scattering of THz radiation, measurements of capacitive response times, picosecond avalanche electron multiplication, and attenuation of TE₁₀ mode in rectangular waveguide; however, these methods yield relative and/or indirect measurements associated with ambiguous interpretation.^{9,25,28,29,30,31,32,33} Direct counting of photoionized electrons based on picosecond avalanche amplification of individual electrons was reported recently and the method is well-suited for very low ionization degrees $\leq 10^{-10}$.³⁴

Recently, coherent microwave scattering (CMS) was demonstrated as an effective diagnostic technique for the measurement of photoionization rates and temporally-resolved electron number densities at laser-induced photoionization in UV and near-IR spectral ranges.^{35,36,37} State-of-the-art CMS systems are associated with high sensitivity and minimal detectable number of electrons in microplasma volume $\sim 10^8$. In this work, we expand CMS application to measure the total electron count and electron number density produced by focusing a 3.9 μm femtosecond laser pulse in air and subsequently determine tunnelling ionization rates of ambient air in the mid-IR spectral band.

Experimental Details and Methodology. - The experiments were conducted at the Ultrafast Laser Group of the Photonics Institute at TU Wien (Austria) with the unique 3.9 μm 30 mJ mid-IR femtosecond OPCPA.^{7,38,39} The coherent microwave scattering (CMS) measurement system was provided by Purdue University (USA) to conduct these experiments. The experimental setup including the femtosecond mid-infrared laser and CMS system used in this work is schematically shown in Figure 1.

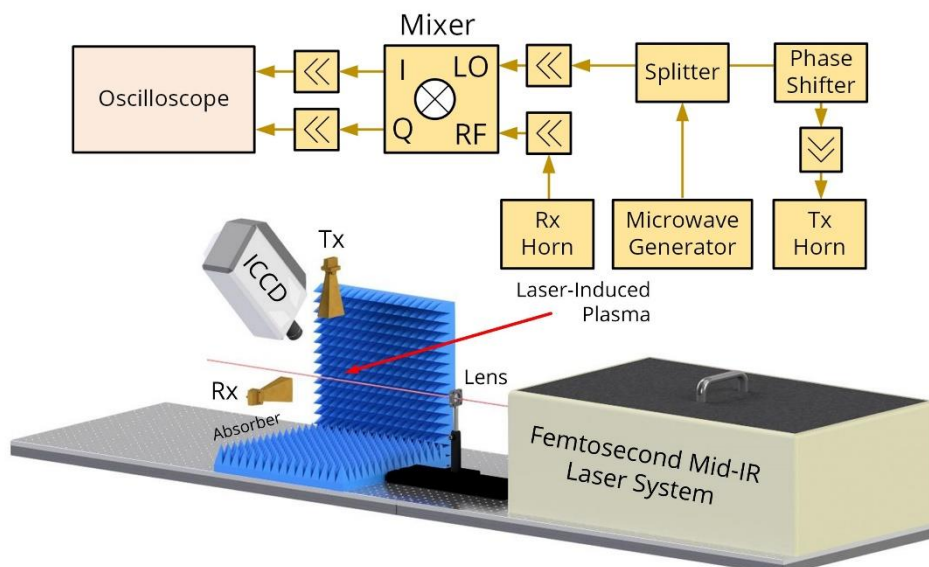


Figure 1. Schematics of the experimental setup containing the 3.9 μm femtosecond laser and coherent microwave scattering system.

Measurements of the total electron count in the laser-induced plasma volume (N_e) and electron number density (n_e) were conducted using a homodyne-type CMS system operating at 11 GHz. Incident

microwave radiation (~ 8 W, Tx horn) was linearly polarized along the plasma channel orientation, and the signal scattered off the plasma volume was received by a microwave horn (Rx horn), amplified, and detected using an I/Q mixer. All components of the microwave system operated in the linear regime to ensure that the measured response is proportional to the amplitude of the scattered signal. The temporal resolution of the CMS system was about 1 ns, limited by 1 GHz bandwidth LeCroy WaveRunner 104Xi oscilloscope used in the circuit. The CMS system was calibrated using Teflon dielectric scatterers and attribution of the measured scattering signal U_S to N_e was done via the following equation:

$$U_S = \begin{cases} A \frac{e^2}{m v_m} N_e & \text{– laser – induced plasma} \\ A V_D \varepsilon_0 (\varepsilon_D - 1) \omega & \text{– dielectric scatterer} \end{cases} \quad \text{Eq. 1}$$

where A – the calibration coefficient of the CMS system (evaluated from the lower equation), V_D and ε_D – the volume and the dielectric constant of the Teflon dielectric scatterer, ε_0 – the dielectric permittivity of vacuum, v_m – the electron-gas collisional frequency, and ω – the circular frequency of the microwave radiation. The laser-induced plasma was imaged using an ICCD camera to observe its evolution with laser pulse energy and determine plasma volume V_p . Spatially-averaged electron number density was determined as $n_e = \frac{N_e}{V_p}$. More details on the CMS technique can be found elsewhere.^{35,36,40}

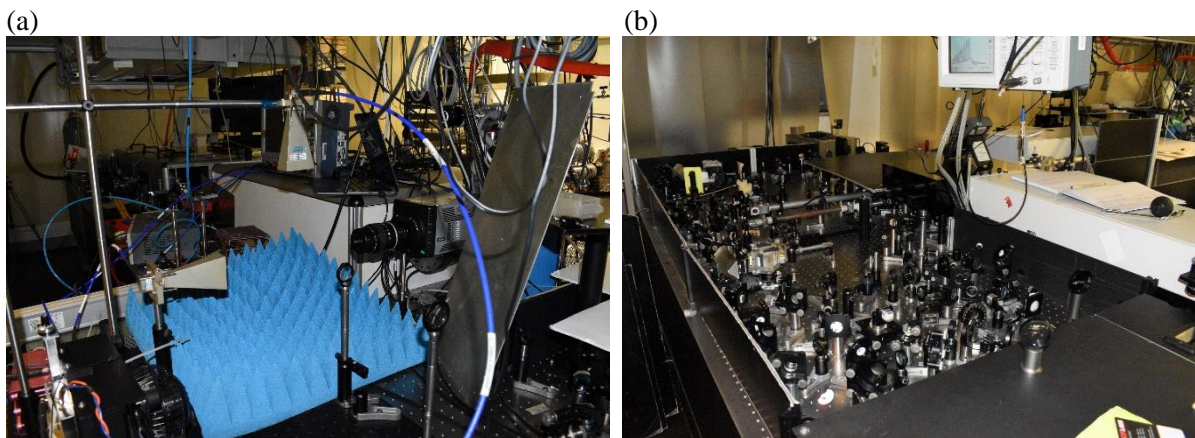


Figure 2. (a) Photograph of CMS system aligned with the beam waist location. (b) Photograph of the 3.9 μm 30 mJ femtosecond laser system.

Results and Discussion. - In the experiments, linearly-polarized 3.9 μm pulses were focused in air by a 150 mm focal length CaF₂ lens. Femtosecond laser pulses were characterized by second-harmonic generation frequency resolved optical-gating (SHG FROG) method, beam-waist was measured by a knife-edge technique (conducted with a strongly attenuated laser beam), and spatial distribution along the propagation was monitored with a Spiricon Pyrocam III beam profiler. The results of these measurements are shown in Figure 3. SHG FROG measurement reveals spectral FWHM – 302.9 nm and temporal FWHM – $\tau_{FWHM}=117.7$ fs. Before focusing, the 3.9 μm beam was slightly elliptical with

the beam diameters in x and y directions at FWHM level being 3.98 mm and 4.64 mm, respectively. The beam waist was evaluated to be $w_0=95.85 \mu\text{m}$. These quantities can be regarded as invariant for the experimental conditions encountered in this work.

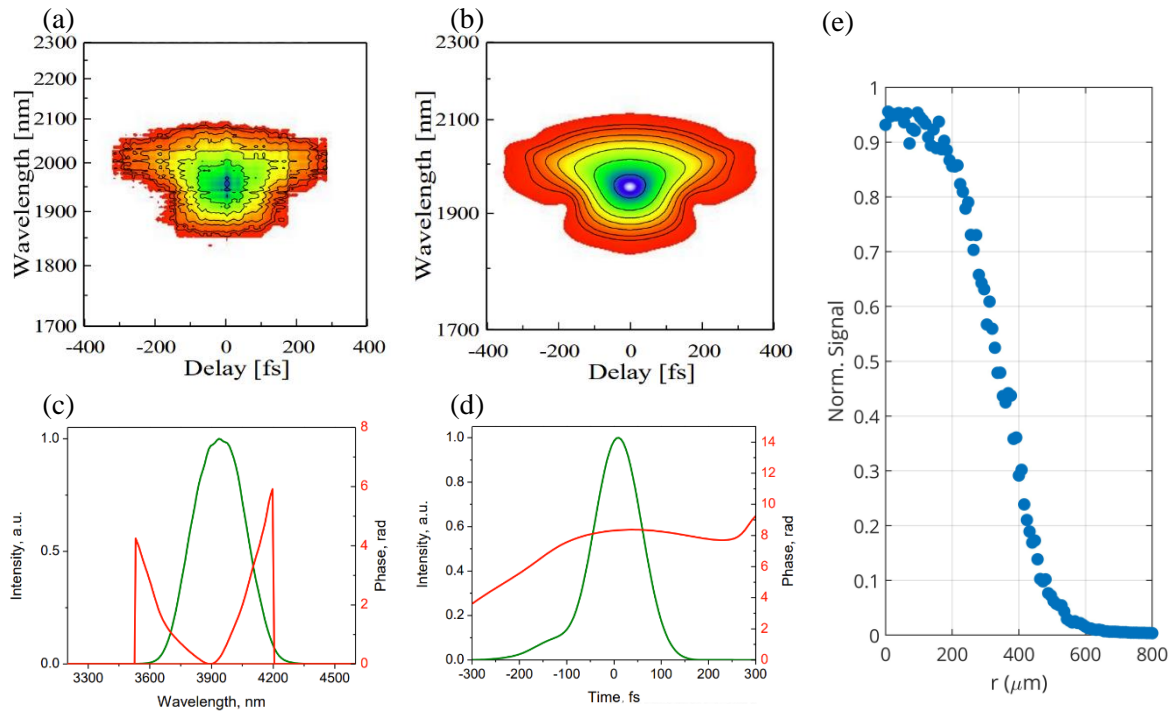


Figure 3. Characteristics of the femtosecond pulse for $E_L = 0.2 \text{ mJ}$. (a) Measured SHG FROG. (b) Retrieved SHG FROG. (c) Spectral composition and phase. (d) Temporal profile and phase. (e) Knife-edge beam waist measurements for $f = 150 \text{ mm}$.

Representative line-of-sight ICCD images (gate width 100 ns) of laser-induced plasmas in ambient air and spatial beam-profiling acquired 15 cm behind the focal plane are depicted in Figure 4 for various laser pulse energies. As observed, and consistent with characteristics of the laser / focusing arrangement, encountered plasma channels are rather short, on the order of a millimeter. One can conclude that beam propagation for the tested irradiating energies E_L up to $\sim 3.5 \text{ mJ}$ can be regarded as nearly linear. This is justified by (1) relative invariance of the laser beam profile and (2) symmetry (longitudinal and transversal) of plasma geometric features up to $E_L \sim 2 \text{ mJ}$ as well as by a fairly weak shift of the focal point in the focusing lens direction. Slight onset of the nonlinear optical effects is encountered at the upper edge of tested energy range $E_L \sim 2\text{-}3.5 \text{ mJ}$. Note that Kerr focusing and plasma defocusing are expected to have comparable magnitude of contributions to the refractive index (n) for the range of tested laser intensities (I_L) and electron number (n_e) densities measured below; namely, $|\Delta n| \approx 5 \times 10^{-5}$ for $I_L = 10^{18} \text{ W/m}^2$ and $n_e = 10^{16} \text{ cm}^{-3}$. Aside, the plasma channel can be regarded as an oblate spheroid with semi-axis estimates of $a = b = 100 \mu\text{m}$ (consistent with knife-edge measurements)

and $c = 0.75$ mm. These dimensions suggest plasma volume $V_p = 3.14 \times 10^{-11} \text{ m}^3$ and somewhat large depolarization factors (governing magnitude of the microwave field screening inside the plasma spheroid due to accumulation of charges on the spheroid ends) on the order of $\xi \approx 0.03$.^{35,36} This, coupled with skin-depth considerations, largely restricts the measurable n_e up to about 10^{22} m^{-3} before a deviation from ideal collisional coherent microwave scattering behavior (and still below the threshold for significant electron-ion Coulomb contributions to ν_m). Note that longitudinal and transversal plasma boundaries determined using ICCD imaging were associated with intensities of about 10% and about 90% of the peak intensity, respectively (for the Gaussian beam with $w_0 = 95.85 \text{ } \mu\text{m}$ and Rayleigh length $z_R = 4.1$ mm). (Even though this result is consistent with our previous work at near-IR, it should be specifically considered/interpreted in the future)³⁶.

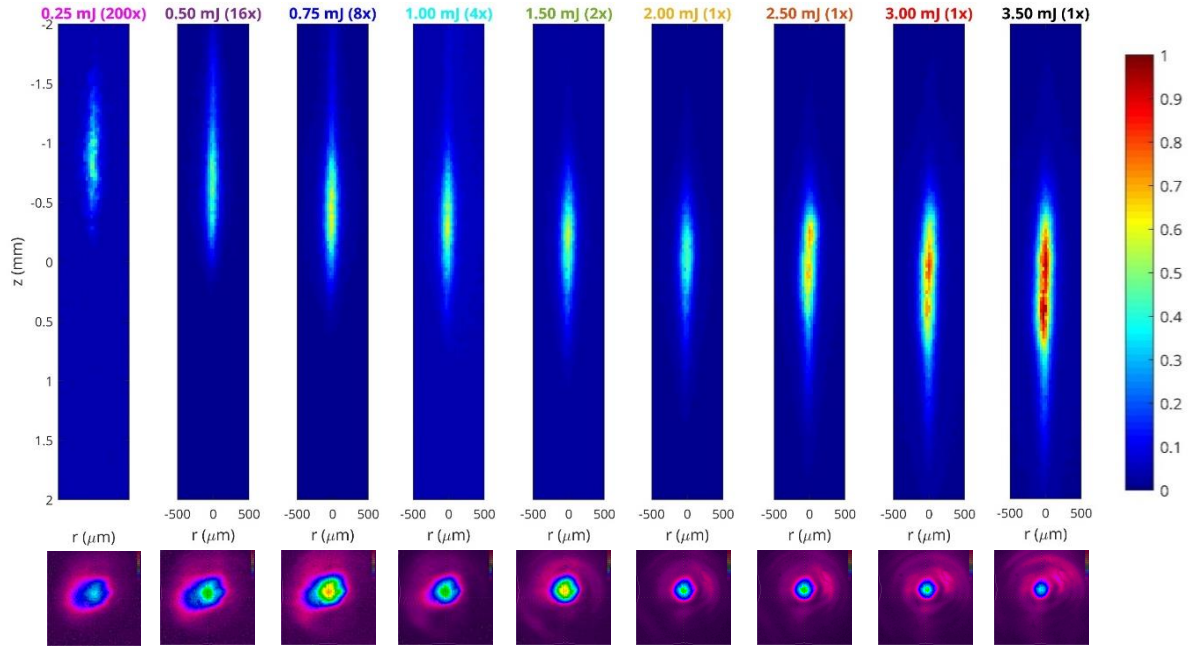


Figure 4. ICCD images (exposure time 100 ns) and spatial beam profiling (acquired 15 cm behind the focal plane) associated with femtosecond mid-infrared photoionization in atmospheric air for irradiating energies E_L up to 3.5 mJ and $f = 150$ mm lens.

Temporal evolution of total electron numbers measured by the CMS is plotted in Figure 5(a) for various E_L (line-colors refer to the headers in Figure 4). N_e was extracted from the measured scattered signal U_s under the assumption of a constant collisional frequency $\nu_m = 2 \cdot 10^{12} \text{ s}^{-1}$ corresponding to an electron temperature of $T_e \sim 1$ eV. This is consistent with quick T_e collapse from the range corresponding to quiver energy ($E_{\sim} = e^2 I_L / 2c \epsilon_0 m_e \omega_L^2 \approx 10 - 100$ eV) to an approximately single eV/sub-eV range on the timescale of $\ll 1$ ns followed by fairly slow evolution during several next ns.²⁸ Note that during this quick T_e -collapse phase the electrons can produce post-pulse ionization of air and, therefore, reported N_e -values might be slightly overestimated (about factor of 2-3). Additionally, observed CMS measurements unrealistically reflect (underestimate) the initial growth

stage of N_e temporal dynamics due to limited temporal resolution of the detecting system of about 1 ns (oscilloscope with 1 GHz bandwidth was used). The decay is governed by dissociative recombination ($X_2^+ + e \rightarrow X + X$, where X is N or O) and three-body attachment to oxygen ($e + O_2 + X_2 \rightarrow O_2^- + X_2$, where X is N or O) and adequately resolved in time by the utilized CMS system.

Temporal evolution of the relative phase of detected microwave radiation measured by the CMS system is plotted in Figure 5(b). One can see that, for all tested pulse energies, the phase quickly collapsed to a constant value and remained unchanged during the subsequent electron decay which is indicative of a collisional scattering regime. This validates the mathematical formulation used to evaluate N_e from the measured scattered signal U_s (upper Eq. 1). Note that pulse energies $E_L > 2\text{mJ}$ might indicate a mixed collisional-Rayleigh scattering regime during first nanosecond after the laser pulse.

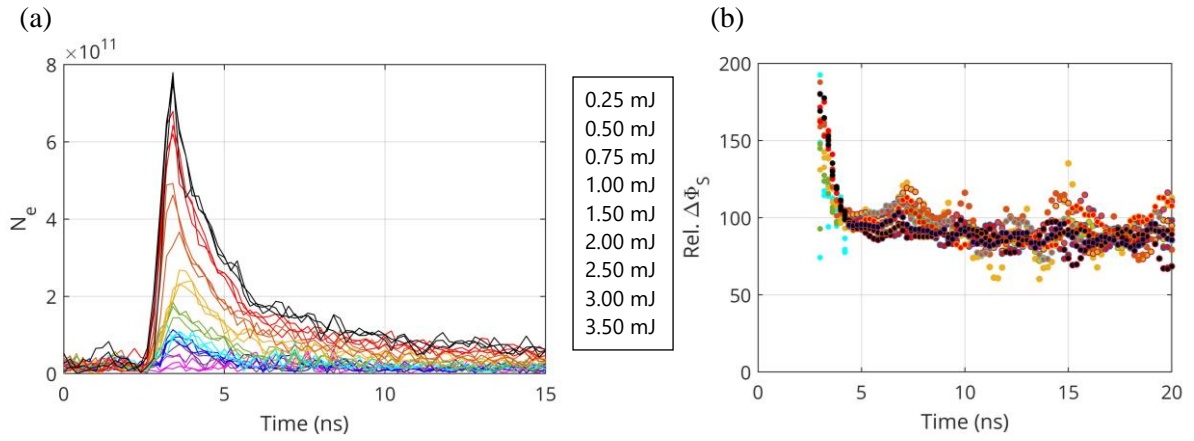


Figure 5. (a) Temporal decay of N_e measured via CMS for various E_L . Line coloring corresponds to the headers in Figure 4. (b) Associated relative phase waveforms.

Spatially averaged electron number density (n_e) and photoionization rate (ν_{PI}) are plotted as a function of laser intensity in Figure 6. n_e was determined as $n_e = \frac{N_e}{V_p}$ and ν_{PI} was subsequently calculated from the simple relation $n_e = n_g \nu_{PI} \tau_{FWHM}$, where n_g is air number density ($n_g = 2.5 \times 10^{25} \text{ m}^{-3}$). Laser intensities indicated on the horizontal axis were calculated assuming Gaussian beam intensity distribution in spatial and temporal domains in vicinity of the waist using $I_L = \frac{E_L}{\frac{1}{2}\pi w_0^2 \tau_{FWHM} \sqrt{\pi}}$. Note that assumption of Gaussian intensity distribution is based on experimentally validated linear beam propagation with weak contribution of nonlinear optical effects as detailed above. It was observed that total electron count N_e scaled with laser energy E_L as $N_e \propto E_L^{(1.5-1.7)}$; however, determination of effective plasma volume based on this scaling law (developed and utilized in our previous works)^{36,37} was not pursued in this work as it was beyond the accuracy of the current dataset associated with limited size and substantial measurement errors.

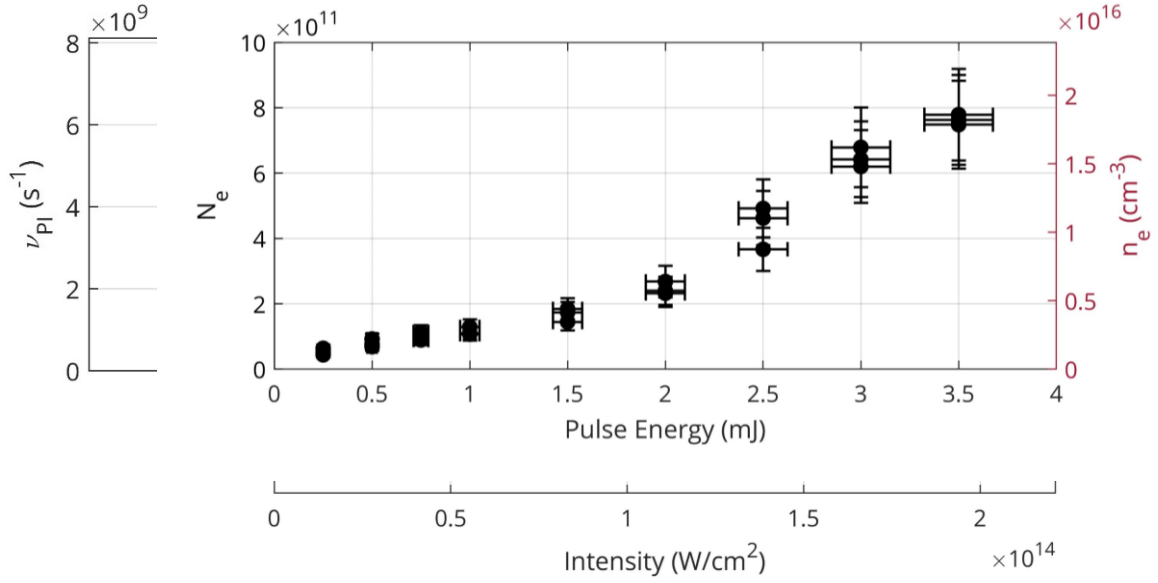


Figure 6. Experimentally-measured total electron numbers, electron number densities, and photoionization rates as a function of pulse energy / peak intensity.

In summary, photoionization rates at 3.9 μm wavelength were experimentally determined for the range of radiation intensities $1.3 \times 10^{13} - 1.9 \times 10^{14} \text{ W/cm}^2$ using 3.9 μm femtosecond laser and absolutely calibrated coherent microwave scattering technique. Several important modifications can be considered in the future to improve accuracy of ν_{PI} determination and extend the intensity range. First, more rigor procedure for identifying effective plasma volume via deriving exact power-law scaling of N_e with E_L , extrapolating the same scaling locally on n_e vs. I_L dependence, and conducting corresponding integrations similar to the methodology developed in our recent works.^{36,37} This would further introduce a correction to the effective plasma volume V_p and, correspondingly, to photoionization rate ν_{PI} . Second, experiments in pure gases should be conducted to identify individual contributions of various gaseous species containing in the atmospheric air (O_2 , N_2 , etc.) to the overall photoionization rate. Note that in current work we calculated ν_{PI} based on the total air density $n_g = 2.5 \times 10^{25} \text{ m}^{-3}$ so that higher gas-specific photoionization rates (e.g., ν_{O_2} , ν_{N_2}) should be expected ($\nu_{PI} = \nu_{\text{O}_2} \chi_{\text{O}_2} + \nu_{\text{N}_2} \chi_{\text{N}_2}$, where χ_{O_2} and χ_{N_2} are mole fractions of oxygen and nitrogen in air). Photoionizations rates measured in this work coincide with the lower bound of the corresponding range predicted by various theoretical models developed in the past ($10^9 - 10^{13} \text{ s}^{-1}$ for the radiation intensity $\sim 10^{14} \text{ W/cm}^2$ with intensity scaling varying in the range $I_L^{(1-5)}$)²⁵. Note that we compare the photoionizations rates measured in this work at 3.9 μm with that reported previously at 800 nm as similar rates in the tunneling regime are expected (largely governed by the amplitude of electric field rather than by the photon energy/wavelength determining the multiphoton regime). Third, conducting

experiments in collisionless ν_m -independent Thomson scattering regime at low pressures ($p \leq 1$ Torr) would allow to substantially extended the range of intensities at which ν_{PI} can be evaluated by delaying the onset of nonlinear optical phenomena to higher laser intensities.³⁵ This refers to the fact that nonlinear optical phenomena including Kerr and plasma nonlinear terms in the refractive index reduce proportionally with a decrease in pressure ($n_2 \propto n_g \propto p$, $\omega_p^2 \propto n_e \propto n_g \propto p$). Forth, expanding bandwidth of the CMS measurement system is recommended to accurately capture temporal dynamics of N_e and fully resolve N_e peak value.

Conclusions. - In this work, total electron count, electron number densities, and photoionization rates were reported for mid-infrared femtosecond tunneling photoionization at 3.9 μm in atmospheric air using absolutely calibrated coherent microwave scattering technique. Utilization of atmospheric pressure limits the highest intensity at which a photoionization rate can be evaluated due to onset of Kerr focusing. To extend this limit to higher intensities, the experiments at low pressures ($p \leq 1$ Torr) in collisionless Thomson scattering regime should be conducted.

Acknowledgements. - Authors would like to thank D. Kartashov and M. N. Slipchenko for valuable discussions. This work was supported by the National Science Foundation (Grant No. 1903415 and No. 1903360).

References

1. Krausz, F. & Ivanov, M. Attosecond physics. *Rev Mod Phys* **81**, 163 (2009).
2. Couairon, A. & Mysyrowicz, A. Femtosecond filamentation in transparent media. *Phys Rep* **441**, 47 (2007).
3. Chin, S. L. *Femtosecond laser filamentation*. (Springer Science, 2010).
4. Polynkin, P. & Cheng, Y. *Air lasing*. (Springer Series in Optical Sciences, 2018).
5. Mitrofanov, A. v. *et al.* Mid-infrared laser filaments in the atmosphere. *Sci Rep* **5**, 8368 (2015).
6. Tochitsky, S. *et al.* Megafilament in air formed by self-guided terawatt long-wavelength infrared laser. *Nat Photonics* **13**, 41 (2019).
7. Shumakova, V. *et al.* Filamentation of mid-IR pulses in ambient air in the vicinity of molecular resonances. *Opt Lett* **43**, 2185 (2018).
8. Schultz, K. D. *et al.* Strong field physics with long wavelength lasers. *J Mod Opt* **54**, 1075 (2007).

9. Mongin, D. *et al.* Conductivity and discharge guiding properties of mid-IR laser filaments. *Applied Physics B* **122**, 267 (2016).
10. Popmintchev, T. *et al.* Bright Coherent Ultrahigh Harmonics in the keV X-ray Regime from Mid-Infrared Femtosecond Lasers. *Science (1979)* **336**, 1287 (2012).
11. Panagiotopoulos, P., Whalen, P., Kolesik, M. & Moloney, J. v. Super high power mid-infrared femtosecond light bullet. *Nat Photonics* **9**, 543 (2015).
12. Woodbury, D. *et al.* Laser wakefield acceleration with mid-IR laser pulses. *Opt Lett* **43**, 1131–1134 (2018).
13. Amico, C. D. *et al.* Forward THz radiation emission by femtosecond filamentation in gases: Theory and experiment. *New J Phys* **10**, 013015 (2008).
14. Wolf, J. P. Short-pulse lasers for weather control. *Reports on Progress in Physics* **81**, 026001 (2018).
15. Kartashov, D., Ališauskas, S., Pugžlys, A., Shneider, M. N. & Baltuška, A. Theory of a filament initiated nitrogen laser. *Journal of Physics B: Atomic, Molecular and Optical Physics* **48**, 094016 (2015).
16. Keldysh, L. v. Ionization in the field of a strong electromagnetic wave. *Soviet Physics JETP* **20**, 1307–1314 (1965).
17. Perelomov, A., Popov, V. & Terent'ev, M. Ionization of Atoms in an Alternating Electric Field. *Soviet Journal of Experimental and Theoretical Physics* **23**, 924 (1966).
18. Ammosov, M. V., Delone, N. B. & Krainov, V. P. Tunnel ionization of complex atoms and of atomic ions in an alternating electromagnetic field. *Soviet Physics - JETP* **664**, 138 (1986).
19. Mur, V. D., Popruzhenko, S. V. & Popov, V. S. Energy and momentum spectra of photoelectrons under conditions of ionization by strong laser radiation (the case of elliptic polarization). *Journal of Experimental and Theoretical Physics* **92**, 777 (2001).
20. Augst, S., Meyerhofer, D. D., Strickland, D. & Chint, S. L. Laser ionization of noble gases by Coulomb-barrier suppression. *Journal of the Optical Society of America B* **8**, 858 (1991).
21. Wahlstrand, J. K., Zahedpour, S., Bahl, A., Kolesik, M. & Milchberg, H. M. Bound-Electron Nonlinearity beyond the Ionization Threshold. *Phys Rev Lett* **120**, 183901 (2018).
22. Litvinyuk, I. V. *et al.* Alignment-Dependent Strong Field Ionization of Molecules. *Phys Rev Lett* **90**, 233003 (2003).
23. Smirnova, O. *et al.* High harmonic interferometry of multi-electron dynamics in molecules. *Nature* **460**, 972 (2009).
24. Tong, X. M., Zhao, Z. X. & Lin, C. D. Theory of molecular tunneling ionization. *Phys Rev A* **66**, 033402 (2002).
25. Talebpour, A., Yang, J. & Chin, S. L. Semi-empirical model for the rate of tunnel ionization of N₂ and O₂ molecule in an intense Ti:sapphire laser pulse. *Opt Commun* **163**, 29 (1999).

26. Walsh, T. D. G., Ilkov, F. A., Decker, J. E. & Chin, S. L. The tunnel ionization of atoms, diatomic and triatomic molecules using intense 10.6 μm radiation. *Journal of Physics B: Atomic, Molecular and Optical Physics* **27**, 3767 (1994).
27. Mishima, K. *et al.* Generalization of Keldysh's theory. *Phys Rev A* **66**, 033401 (2002).
28. Aleksandrov, N. L. *et al.* Decay of femtosecond laser-induced plasma filaments in air, nitrogen, and argon for atmospheric and subatmospheric pressures. *Phys Rev E* **94**, 013204 (2016).
29. Ovsyannikov, A. A. & Zhukov, M. F. *Plasma Diagnostics*. (Cambridge International Science Publishing, 2000).
30. Ionin, A. A. *et al.* Triggering and guiding electric discharge by a train of ultraviolet picosecond pulses combined with a long ultraviolet pulse. *Appl Phys Lett* **100**, 104105 (2012).
31. Fischer, R. P. *et al.* Conductivity measurements of femtosecond laser-plasma filaments. *IEEE Transactions on Plasma Science* **35**, 1430 (2007).
32. Polynkin, P. Mobilities of O^{2+} and O^{2-} ions in femtosecond laser filaments in air. *Appl Phys Lett* **101**, 164102 (2012).
33. Papeer, J. *et al.* Microwave diagnostics of femtosecond laser-generated plasma filaments. *Appl Phys Lett* **99**, 141503 (2011).
34. Woodbury, D., Schwartz, R. M., Rockafellow, E., Wahlstrand, J. K. & Milchberg, H. M. Absolute Measurement of Laser Ionization Yield in Atmospheric Pressure Range Gases over 14 Decades. *Phys Rev Lett* **124**, 013201 (2020).
35. Patel, A. R. *et al.* Thomson and collisional regimes of in-phase coherent microwave scattering off gaseous microplasmas. *Sci Rep* **11**, 23389 (2021).
36. Sharma, A. *et al.* Counting the electrons in a multiphoton ionization by elastic scattering of microwaves. *Sci Rep* **8**, 2874 (2018).
37. Sharma, A., Slipchenko, M. N., Rahman, K. A., Shneider, M. N. & Shashurin, A. Direct measurement of electron numbers created at near-infrared laser-induced ionization of various gases. *J Appl Phys* **125**, 193301 (2019).
38. Andriukaitis, G. *et al.* 90 GW peak power few-cycle mid-infrared pulses from an optical parametric amplifier. *Opt Lett* **36**, 2755–2757 (2011).
39. Shumakova, V. Filamentation and Self-Compression of Multi-mJ fs Mid-Infrared Pulses. (TU Wien, 2018).
40. Shneider, M. N. & Miles, R. B. Microwave diagnostics of small plasma objects. *J Appl Phys* **98**, 033301 (2005).